Nanoscale

PAPER

View Article Online
View Journal | View Issue

Cite this: *Nanoscale*, 2016, **8**, 13352

Cell membrane penetration and mitochondrial targeting by platinum-decorated ceria nanoparticles†

Adriano A. Torrano,[a,b] Rudolf Herrmann,[c] Claudia Strobel,[d] Markus Rennhak,[c] Hanna Engelke,[a] Armin Reller,[e] Ingrid Hilger,[d] Achim Wixforth[b,c] and Christoph Bräuchle*[a,b]

Received 27th November 2015,
Accepted 10th June 2016

DOI: 10.1039/c5nr08419a

www.rsc.org/nanoscale

In this work we investigate the interaction between endothelial cells and nanoparticles emitted by catalytic converters. Although catalyst-derived particles are recognized as growing burden added to environmental pollution, very little is known about their health impact. We use platinum-decorated ceria nanoparticles as model compounds for the actual emitted particles and focus on their fast uptake and association with mitochondria, the cell's powerhouse. Using live-cell imaging and electron microscopy we clearly show that 46 nm platinum-decorated ceria nanoparticles can rapidly penetrate cell membranes and reach the cytosol. Moreover, if suitably targeted, these particles are able to selectively attach to mitochondria. These results are complemented by cytotoxicity assays, thus providing insights into the biological effects of these particles on cells. Interestingly, no permanent membrane disruption or any other significant adverse effects on cells were observed. The unusual uptake behavior observed for 46 nm nanoparticles was not observed for equivalent but larger 143 nm and 285 nm platinum-decorated particles. Our results demonstrate a remarkable particle size effect in which particles smaller than ~50–100 nm escape the usual endocytic pathway and translocate directly into the cytosol, while particles larger than ~150 nm are internalized by conventional endocytosis. Since the small particles are able to bypass endocytosis they could be explored as drug and gene delivery vehicles. Platinum-decorated nanoparticles are therefore highly interesting in the fields of nanotoxicology and nanomedicine.

1. Introduction

Particle pollution is made up of extremely small liquid droplets and solid particles from a variety of components, including acids, organic compounds, soot, dust and metals.[1] Exposure to particle pollution has been associated with a number of respiratory, cardiovascular and neurologic diseases.[2–5] Notably, particle pollution has recently been classified as carcinogenic to humans,[6] and outdoor air pollution has been pointed as a leading cause of cancer deaths.[7] With regard to the size distribution in the ambient atmospheric environment, particles <300 nm represent more than 99% of the total number concentration.[8] Globally, the main source of nano-sized particles in urban air is motor traffic.[3,9]

In order to mitigate the emission of particles and other dangerous substances from the engine, modern vehicles are equipped with catalytic converters. Automobile catalytic converters are able to transform more than 90% of total unburned hydrocarbons, carbon monoxide, and nitrogen oxides into rather harmless compounds, such as carbon dioxide, nitrogen and water. On the whole, they consist of a porous carrier material (*e.g.* CeO_2, or ceria) that is decorated with active noble metals (normally platinum, but also palladium and rhodium). Although playing a fundamental role in reducing the emission of pollutants from vehicles, catalytic converters decompose with time and generate new particle emissions in the nano- and micrometer ranges. Catalyst-derived particles consisting of a carrier material and decorated with noble metals are thus formed and released into the environment.[10–17] As a result of

[a]*Department of Chemistry and Center for NanoScience (CeNS), University of Munich (LMU), 81377 Munich, Germany. E-mail: christoph.braeuchle@cup.uni-muenchen.de*
[b]*Nanosystems Initiative Munich (NIM), 80799 Munich, Germany*
[c]*Experimental Physics I, Institute of Physics, University of Augsburg, 86159 Augsburg, Germany*
[d]*Department of Experimental Radiology, Institute of Diagnostic and Interventional Radiology, Jena University Hospital – Friedrich Schiller University Jena, 07747 Jena, Germany*
[e]*Resources Strategy, Institute of Physics, University of Augsburg, 86159 Augsburg, Germany*

†Electronic supplementary information (ESI) available: Further information on the characterization of nanoparticles and additional live-cell imaging studies. See DOI: 10.1039/c5nr08419a

the escalating traffic worldwide, the concentration of noble metals (free or bound to the carrier material) has been increasing in urban areas. Wichmann *et al.*[17] reported that the concentration of catalyst-derived platinum in the air of Braunschweig City (Germany) jumped from 6.0 pg m^{-3} in 1999 to 159 pg m^{-3} in 2005. Nanoparticles (NPs) generated by catalytic converters are therefore a growing burden added to particle pollution.

Since very little is known about the health impact of catalyst-derived NPs, our goal in this work is to investigate the biological effect of these NPs at the cellular level. Studying the interaction of catalyst-derived NPs with biological systems directly is hardly possible due to the low concentrations in samples like road dust. For this purpose, reasonable quantities of model compounds that resemble the actual catalyst-derived NPs were synthesized.[18] Our mimetic compounds consist of a ceria NP core (defined sizes between 8 and 285 nm) decorated with ultrasmall platinum NPs (2–5 nm). The interaction between platinum-decorated ceria nanoparticles (Pt-ceria NPs) and human microvascular endothelial cells (HMEC-1) was studied in detail by live-cell imaging. Inhalation, skin contact, and ingestion are the main routes for NPs to enter the human body.[19] In all three cases NPs can reach the bloodstream, where they can interact with endothelial cells covering the inner surface of blood vessels.[20,21] These cells play a crucial role in the process of blood flow, while changes in endothelium are often found in a number of diseases.[22–25] Therefore, endothelial cell lines represent an important model system to investigate the bioactivity and cellular uptake of NPs. In addition, we investigated if the same uptake behavior would be found in other cell types, such as human cervical cancer cells (HeLa). Surprisingly, Pt-ceria NPs of specific characteristics were rapidly found inside living cells and selectively associated with mitochondria. These exciting findings focused our investigations on the biological effects related to the unusual fast NP uptake mechanism as well as the mitochondrial-targeting properties of the model compounds.

Several mechanisms for the cellular uptake *via* endocytosis have been discussed in the literature. The most relevant and better understood mechanisms are clathrin-mediated endocytosis, caveolin-mediated endocytosis, macropinocytosis, and phagocytosis.[26–28] Interestingly, cell-penetrating peptides,[29] CdSe/ZnS core/shell quantum dots (8 nm, coated with D-penicillamine),[30] and ultrasmall noble metal NPs (typically smaller than ~10 nm), such as gold,[31–35] and platinum,[36,37] can escape the traditional endocytosis pathway and perform a fast direct translocation across the cell membrane into the cytosol. This unconventional uptake mechanism is characterized by fast and efficient cellular uptake, no perceptible cell membrane disruption and low cytotoxic effects.[31] Although often reported, the mechanism of cell membrane penetration is not fully understood. Using coarse-grained molecular dynamics simulations, Lin and Alexander-Katz[31] proposed that cell membranes generate nanoscale transient holes to assist the fast and spontaneous translocation of cell-penetrating peptides as well as ultrasmall cationic NPs into the cytoplasm. According to this model, when ultrasmall cationic NPs (*e.g.* 2.2 nm gold particles) approach the membrane, they are attracted to negatively charged membrane proteins. Once a certain number of NPs are located in the membrane region, nanoscale holes are formed due to the alteration of the local electric field across the plasma membrane. NPs that are already in the region will then use these holes to directly translocate into the cytosol. After translocation, the transmembrane potential is strongly reduced and the membrane rapidly reseals itself. In this context, delivery of payloads by NPs that are able to rapidly enter cells and accumulate in organelles has great potential to advance the treatment of many disorders. The interaction of Pt-ceria NPs with cells is therefore highly interesting with respect to the two complementary fields of nanotoxicology and nanomedicine. On the one hand, it plays an important role in the toxicology of nanomaterials and particle pollution; on the other hand, it can help to deliver therapeutics directly to mitochondria in the field of drug delivery and nanomedicine.

2. Results and discussion

2.1 Characterization of Pt-ceria NPs

A reproducible method for the synthesis of platinum-decorated ceria NPs that resemble those emitted from catalytic converters was developed and published in the literature by Herrmann *et al.*[18] Basically, the model compounds are made up of a ceria NP core of defined sizes (between 8 and 285 nm) decorated with ultrasmall platinum NPs (2–5 nm). Particles are labeled with covalently-bound fluorophores (Atto 647N or perylenediimide) to allow the detection by fluorescence microscopy techniques. Labeling was performed with modified dyes containing triethoxysilyl groups. These groups react and form covalent bonds with the hydroxyl moieties commonly present at the surface of ceria and other oxidic nanoparticles.[18] The fluorescent dye precursor (size <2 nm) is thus connected to terminal OH groups at the CeO_2 surface through a transesterification reaction.

The size and shape of the model compounds synthesized for our investigations were characterized by transmission electron microscopy (TEM) measurements. Fig. 1 shows the TEM images of 8 nm ceria NPs decorated with platinum and labeled with Atto 647N (Pt-Ceria-8-atto). The primary particle size was determined by image analysis of TEM micrographs. In addition, energy-dispersive X-ray (EDX) spectroscopy (Fig. 1C) was used to prove the elemental composition of the model particles, with platinum (in blue) deposited on ceria NP cores (cerium in red).

Airborne NPs, like those released by automobile catalytic converters, tend to form aggregates in the nano- and micrometer ranges. A comparable tendency towards aggregation was observed during the synthesis of our model compounds. Large and irregular aggregates of Pt-Ceria-8-atto NPs of different sizes and shapes can be easily identified in Fig. 1.

The aggregation of particles was further characterized by dynamic light scattering (DLS) measurements of NPs dispersed in ethanol, the solvent in which particles were synthesized, as well as in cell medium supplemented with 10% FBS (fetal

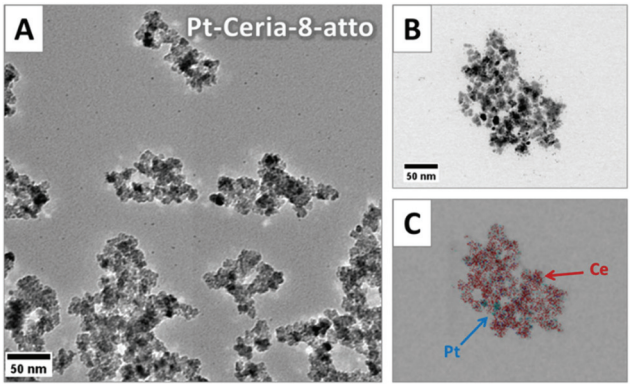

Fig. 1 TEM and EDX images of 8 nm ceria NPs decorated with platinum (Pt-Ceria-8-atto). (A) Electron micrograph of Pt-Ceria-8-atto NPs. Strong aggregation of model compounds resembling the actual catalyst-derived NPs found in the environment. (B) Representative aggregate of Pt-Ceria-8-atto NPs. (C) EDX mapping of the same region in (B). This technique was used to confirm the deposition of platinum (blue) on ceria NP cores (red).

bovine serum). DLS measurements of the Pt-Ceria-8-atto NPs revealed a mean hydrodynamic diameter of 129 nm in ethanol and 246 nm in cell medium, with relatively broad size distributions (PDIs = 0.121 and 0.258, respectively). Analogous model compounds of 8 nm Pt-ceria NPs were prepared and labeled with a perylenediimide-derived dye with a triethoxysilyl anchor group (sample Pt-Ceria-8-pery).[18] The mean hydrodynamic size of the Pt-Ceria-8-pery NPs was determined to be 154 nm (PDI = 0.116) in ethanol and 229 nm in cell medium (PDI = 0.506). The results are summarized in Table 1.

On the one hand, it is desirable to investigate the interaction of model compounds that closely resemble not only the composition but also the aggregation behavior of actual catalyst-derived NPs. On the other hand, it is of paramount importance to find out whether model compounds of different sizes would have distinct biological effects. Ideal samples to investigate particle-size dependent cellular responses should thus have very narrow size distributions. To accomplish this task we developed a strategy to synthesize Pt-ceria NP samples with reasonable monodisperse size distributions (*i.e.* PDI <0.1). The method is based on using polyvinylpyrrolidone (PVP), a surface-active reagent, to obtain the aggregation control of 8 nm ceria NPs during the synthesis.[18] This means that NP aggregation is not avoided, but rather controlled. Fig. 2 shows representative TEM images of stable, uniform and almost spherical aggregates achieved by using this strategy. Ceria NPs of 8 nm are the building blocks to form new NPs of 47 nm (Ceria-47-atto, Fig. 2A). Nearly spherical ceria NP aggregates are the ideal starting material for mimetic catalyst-derived NPs

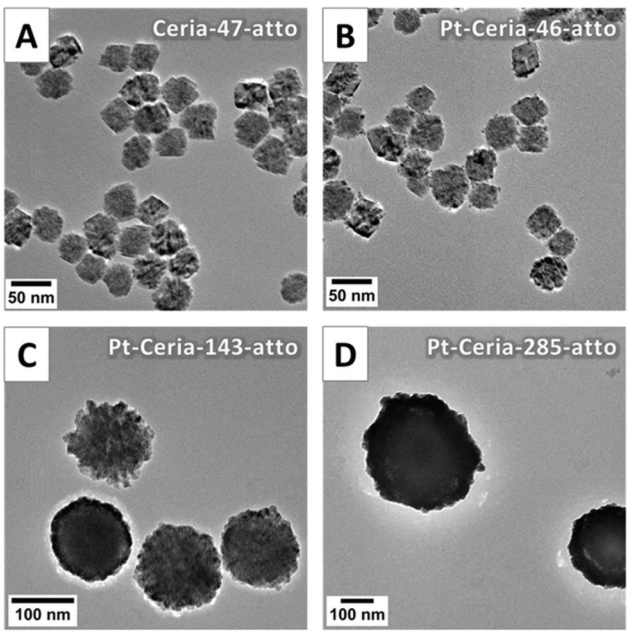

Fig. 2 TEM images of ceria and Pt-ceria NPs of different sizes. Electron micrographs of (A) non-decorated ceria NPs with a mean size of 47 nm, (B) platinum-decorated ceria NPs of 46 nm, (C) 143 nm, and (D) 285 nm.

Table 1 Characterization of ceria and Pt-ceria NPs used in this study

Particle	Fluorescent dye	Primary particle size[a] [nm]	Aggregate size[a] [nm]	Hydrodynamic size[b] [nm]		PDI[e]		Zeta potential [mV]	
				EtOH[c]	Cell medium[d]	EtOH[c]	Cell medium[d]	EtOH[c]	Cell medium[d]
Pt-Ceria-8-atto	Atto 647N	8	n.d.[f]	129	246	0.121	0.258	+35.1	−7.6
Pt-Ceria-8-pery	Perylenediimide	8	n.d.[f]	154	229	0.116	0.506	+27.1	−10.8
Ceria-47-atto	Atto 647N	8	47	110	158	0.096	0.486	+36.4	−6.5
Pt-Ceria-46-atto	Atto 647N	8	46	103	135	0.157	0.372	+45.9	−7.4
Pt-Ceria-143-atto	Atto 647N	8	143	167	173	0.020	0.340	+35.3	−10.0
Pt-Ceria-285-atto	Atto 647N	8	285	292	428	0.060	0.172	+49.2	−10.6

[a] Particle diameter measured by transmission electron microscopy (TEM). [b] Mean hydrodynamic diameter determined by dynamic light scattering (DLS) measurements. [c] Particle dispersion in ethanol. [d] Particle dispersion incubated for 30–40 min in cell medium supplemented with 10% FBS. [e] Polydispersity index (PDI) is a width parameter describing the hydrodynamic particle size distribution. Shortly, PDI <0.1 indicates monodisperse samples with narrow size distributions, PDI between 0.1 and 0.5 characterizes a relatively broad size distribution, and PDI >0.5 points to polydisperse samples with broad size distributions. [f] Not determined.

of defined core sizes and decorated with platinum. By using this procedure, Pt-decorated ceria NPs of three different core sizes were produced: 46 nm (Pt-Ceria-46-atto), 143 nm (Pt-Ceria-143-atto), and 285 nm (Pt-Ceria-285-atto). The TEM images of these particles are shown in Fig. 2B–D, respectively.

DLS measurements revealed the hydrodynamic diameter and the PDI values of the new samples. The results presented in Table 1 show that reasonable narrow size distributions were achieved. Ceria-47-atto and Pt-Ceria-46-atto, the smaller model compounds, still presented a tendency to increase their sizes by clustering with neighboring aggregates in a process that can be termed super-aggregation (Fig. 2A and B). This is directly reflected by the mean hydrodynamic sizes/PDI of these samples dispersed in ethanol: 110 nm/0.096 for Ceria-47-atto NPs and 103 nm/0.157 for Pt-Ceria-46-atto NPs. Even more satisfactory results were obtained with the larger model compounds Pt-Ceria-143-atto and Pt-Ceria-285-atto. Very small PDI values were achieved and the mean hydrodynamic sizes were just slightly larger than those measured by TEM (as expected, due to hydration and solvation effects). The mean hydrodynamic sizes/PDI in ethanol were determined to be 167 nm/0.020 for Pt-Ceria-143-atto NPs and 292 nm/0.060 for Pt-Ceria-285-atto NPs.

The transfer of ceria and Pt-ceria NPs from ethanol into cell medium, while avoiding the formation of large aggregates and super-aggregates, was a considerable challenge. In many cases, the traditional method to redisperse NPs (centrifugation followed by washing steps and a final redispersion in water) failed completely. Using this procedure, aggregates in the micrometer range were often formed and could not be broken down again to the original particle sizes. Importantly, in such cases cell membrane penetration by aggregated Pt-ceria NPs was not detected. In fact, this was the first hint that led us to explore the strong particle size-dependent effect in the uptake behavior of Pt-ceria NPs. After innumerous trials with different conditions and methods, an efficient and yet simple procedure was designed. Shortly, a small aliquot of well-dispersed NPs in ethanol is added into a microreaction tube; ethanol is left to evaporate; dried NPs are then redispersed directly in cell medium (see details in section 3.2). The final NP dispersion in cell medium, prepared as just described, maintained the particles closer to their original sizes. Importantly, NPs smaller than ~50–100 nm were still present after redispersion, as indicated overall by the remarkable and consistent particle-size dependent uptake behavior of Pt-ceria NPs.

The surface charge, or zeta potential, of all samples dispersed in either ethanol (after synthesis) or in cell medium supplemented with 10% FBS was determined based on electrophoretic mobility measurements (Table 1). Positive surface charges with comparable magnitudes were measured in all samples dispersed in ethanol, with values ranging from +27.1 mV for Pt-Ceria-8-pery NPs to +49.2 mV for Pt-Ceria-285-atto NPs. The zeta potential values of all samples dispersed in cell medium were also found to be similar to each other, with negative values ranging from −10.8 mV for Pt-Ceria-8-pery to −6.5 eV for Ceria-47-atto. These results indicate that zeta potential values were not considerably altered by labeling, platinum decoration, or differences in the primary particle size. Therefore, all samples used in this study have a comparable net surface charge that, as expected, will mainly depend on the dispersion medium.

2.2 Uptake kinetics and intracellular fate of Pt-ceria NPs

The cellular uptake of catalyst-derived model NPs was investigated by live-cell imaging. Basically, endothelial cells (HMEC-1) were incubated with cell culture medium containing 20–100 μg mL^{-1} of ceria or Pt-ceria NPs under controlled conditions and imaged live afterwards.

The very first uptake experiments in which HMEC-1 cells were incubated with Pt-Ceria-8-atto NPs revealed remarkable results: NPs were rapidly internalized by cells and were found selectively attached to mitochondria. As depicted in Fig. 3A, a substantial amount of Pt-Ceria-8-atto NPs is found associated with mitochondria after just 10 min of incubation time. Determination of Manders' overlap coefficient[38] revealed that as much as 91% of NPs overlap the mitochondria. Time-lapse confocal live-cell studies confirmed the association of NPs with mitochondria. In Fig. 3B, the typical dynamics of mitochondria inside cells can be appreciated. The translational motion and the bending of mitochondria are exactly followed by associated NPs, resulting in a perfect colocalization in space and time (see movie available as ESI "movie_mt-NPs"†).

Interestingly, traditional endocytosis does not seem to be the uptake pathway taken by Pt-Ceria-8-atto NPs after short incubation times. In the live-cell imaging study presented in Fig. 4A, the cell plasma membrane was stained just before the addition of NPs. Thus, new endosomes formed from the cell surface (possibly enclosing NPs) were fluorescently marked. Our results consistently showed no endosomal localization of Pt-Ceria-8-atto NPs (here, only 1% of the NP signal overlaps endosomes). The particles were instead distributed along with the filament-like structures of the mitochondrial network, as elucidated in Fig. 3. After relatively long incubation times, however, the results were different. The peculiar uptake behavior of the Pt-Ceria-8-atto NPs after 18 h of incubation time is shown in Fig. 4B. Pt-ceria NPs do not only accumulate in mitochondria but also in lysosomes, the terminal vesicles that receive the cargo from endosomes.[39] On the whole, a mixed uptake pathway was observed. Our findings points to the presence of two populations of particles in the sample: one population that escapes the endocytic pathway, is rapidly internalized, and accumulates in mitochondria; and another population that follows traditional endocytosis, is less efficiently internalized, and is delivered to lysosomes. Further research has demonstrated that particle size is a crucial factor determining the uptake mechanism of Pt-ceria NPs (see below).

2.3 Mitochondrial targeting

As already emphasized, not only the fast NP uptake was remarkable, but also the efficient and selective mitochondrial targeting by Pt-Ceria-8-atto NPs. Targeting mitochondria with

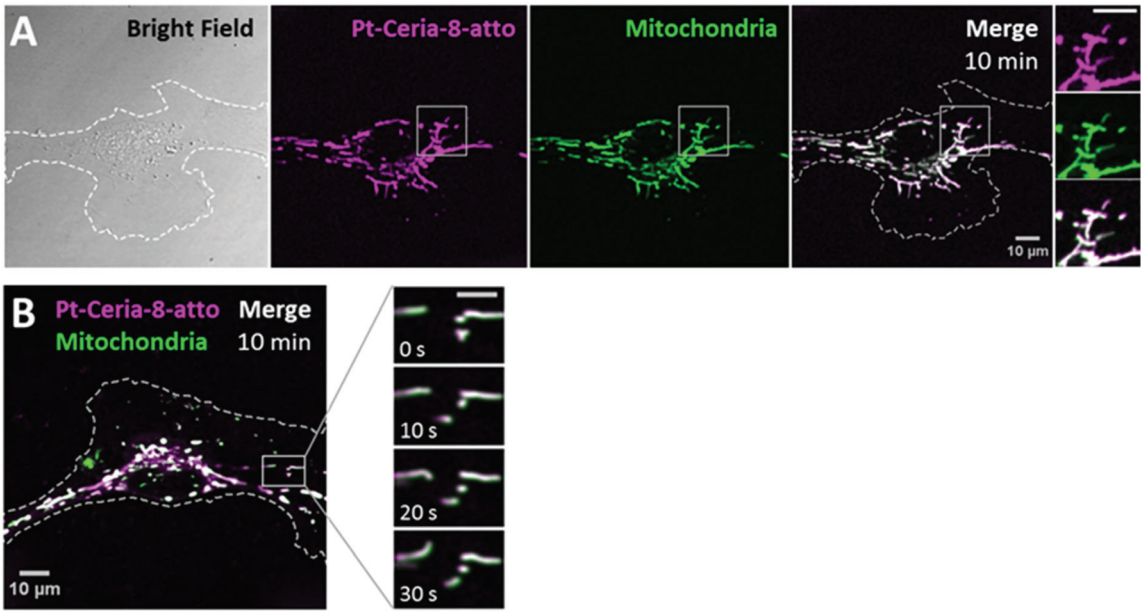

Fig. 3 Live-cell imaging studies on the cellular uptake behavior of Pt-Ceria-8-atto NPs during a short interaction time. (A) Bright-field (left panel) and confocal images of a representative HMEC-1 cell (dashed line) incubated with Pt-Ceria-8-atto NPs for 10 min. After this short period, a considerable number of NPs (middle left panel, magenta) were internalized and accumulated in mitochondria (middle right panel, green: MitoTracker). Note the high degree of colocalization (Manders' overlap coefficient of 91%) in the merge image (right panel, white). Inset: boxed regions of confocal images in detail. Remarkably, the mitochondrial network and the distribution of Pt-Ceria-8-atto NPs are characterized by overlapping filament-like structures. Scale bar = 10 µm. (B) Confocal image of another representative HMEC-1 cell with Pt-Ceria-8-atto NPs (magenta) associated with mitochondria (green; colocalizing pixels in white). Inset: time-lapse images of the boxed region. Note that the typical mitochondrial dynamics (*e.g.* translational motion, bending, stretching) is perfectly followed by associated NPs with a complete colocalization in space and time (see the ESI "movie_mt-NPs"†). Scale bar = 5 µm. Altogether, these results point to a very fast cellular uptake mechanism of Pt-Ceria-8-atto NPs, followed by a selective NP attachment to mitochondria.

lipophilic cations, such as triphenylphosphonium, has been shown to be a successful strategy.[40,41] Due to the large mitochondrial membrane potential, lipophilic cationic moieties are attracted by and accumulate in mitochondria. Interestingly, Atto 647N is also a lipophilic cationic dye with affinity to mitochondria.[42]

In order to investigate if the mitochondrial-targeting properties observed for Pt-Ceria-8-atto NPs are an intrinsic ability of Pt-ceria NPs, regardless of the attached fluorophores, we prepared 8 nm Pt-ceria NPs labeled with perylenediimide (Pt-Ceria-8-pery), a neutral and chemically quite inert fluorescent dye.[18] Missing the mitochondrial-targeting moieties, perylenediimide-labeled NPs would still be able to perform rapid cell membrane penetration, but would not accumulate selectively in mitochondria. Our hypothesis was confirmed by live-cell confocal studies. HMEC-1 cells were incubated with cell culture medium containing 50 µg mL^{-1} of either Pt-Ceria-8-atto or Pt-Ceria-8-pery NPs for 2 h. Cells exposed to 50 µg mL^{-1} of Pt-Ceria-8-pery NPs presented a blurry cytosolic distribution of NPs. In order to enhance the effect and optimize the visualization, the concentration of the Pt-Ceria-8-pery NPs was increased to 500 µg mL^{-1}. As depicted in Fig. 5, both Pt-Ceria-8-atto and Pt-Ceria-8-pery NPs were internalized by cells, but while Atto 647N-labeled particles are mostly accumulated in mitochondria, perylenediimide-labeled particles are clearly distributed throughout the cytosol. The fraction of Pt-Ceria-8-atto NPs overlapping mitochondria for the upper cell in Fig. 5A is 86%. In contrast, the fraction of the Pt-Ceria-8-pery NPs overlapping mitochondria for the cell on the right in Fig. 5B is 46%. Nevertheless, since perylenediimide-labeled NPs cover the entire cytosolic region, 46% may be an overestimation caused by the diffraction-limited signal of NPs that are not physically associated with mitochondria, but rather diffusely surrounding them. The Atto 647N dye has therefore two functions in our model NPs: labeling and mitochondrial targeting.

This comparison study indicates that only with the assistance of a mitochondrial-targeting moiety (here, Atto 647N) the selective mitochondrial localization of cytosolic NPs is promoted. Since fluorescence microscopy relies on the use of fluorophores to label the objects of interest, eventual dye leakage or dye transfer to other objects may lead to misleading interpretations. It is therefore worth emphasizing why the findings presented in this work cannot be attributed to dye leakage from NPs. First of all, perylenediimide and Atto 647N are covalently bonded to the particle surface.[18] Second, we simulated the leakage of the Atto 647N dye from NPs in the cell medium under comparable live-cell imaging conditions. The outcomes were that free Atto 647N molecules are not able to efficiently cross the plasma membrane of cells, and no accumulation of the Atto 647N dye in the mitochondria was

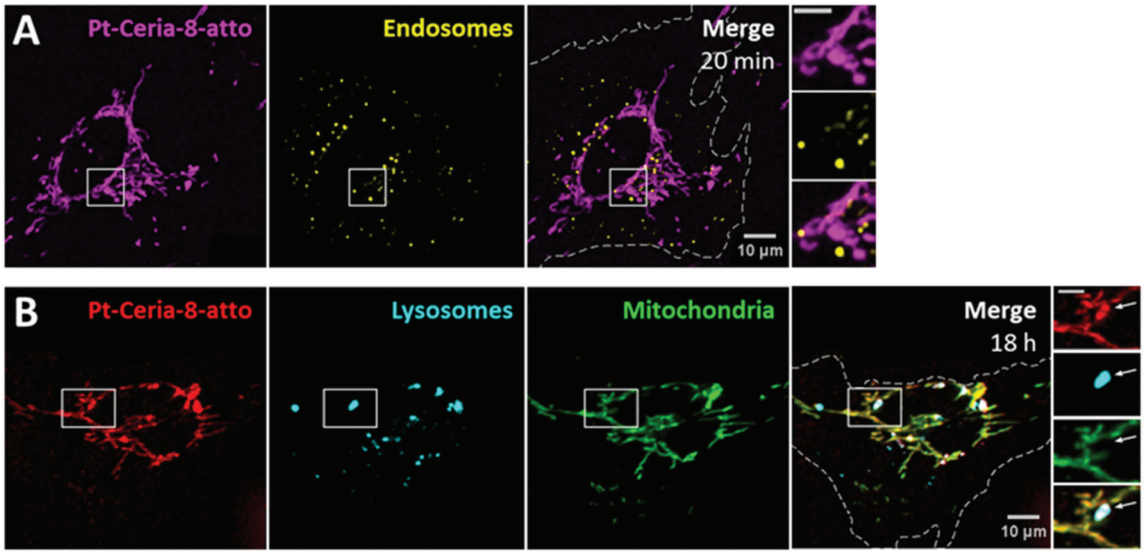

Fig. 4 Intracellular fate of Pt-Ceria-8-atto NPs after short and long interaction times. (A) Live-cell confocal images of a HMEC-1 cell (dashed line) incubated with Pt-Ceria-8-atto NPs (left panel, magenta) for 20 min. Endosomes formed from the cell surface during the interaction with NPs were fluorescently labeled (middle panel, yellow: WGA 488). Large amounts of Pt-ceria NPs were promptly internalized, and colocalization between NPs and endosomes would mean an endocytic entry route. However, this does not seem to be the case for short incubation times, as illustrated in the merge image (right panel, Manders' overlap coefficient of only 1%). Inset: boxed regions in detail. Endosomes form a punctuate pattern, while Pt-Ceria-8-atto NPs are distributed in the characteristic filament-like structures of the mitochondrial network. Note the lack of endosomal localization of NPs. Scale bar = 5 μm. (B) Parallel experiments in which HMEC-1 cells (dashed line) were incubated with Pt-Ceria-8-atto NPs (left panel, red) for 18 h. Cellular lysosomes (middle left panel, cyan: LysoTracker) and mitochondria (middle right panel, green: MitoTracker) were stained before imaging. Interestingly, some Pt-Ceria-8-atto NPs were accumulated in lysosomes (right panel, colocalizing pixels in white), while others in mitochondria (right panel, colocalizing pixels in yellow). Inset: boxed regions in detail. The filament-like structures of NPs associated with mitochondria can be distinguished from the punctuate pattern of those NPs with lysosomal localization (arrow). Scale bar = 5 μm.

observed (Fig. S1†). Finally, equivalent NPs lacking the decoration with platinum or larger than ~150 nm do not display any mitochondrial localization, although labeled with Atto 647N (see below).

2.4 Influence of platinum decoration

An effective investigation on the influence of only platinum decoration requires NPs of similar properties, except for the presence of platinum. For this purpose, we prepared the samples Ceria-47-atto and Pt-Ceria-46-atto. They were synthesized under aggregation control conditions and hold similar properties (Table 1).

HMEC-1 cells were incubated with cell media containing 20 μg mL^{-1} of either Ceria-47-atto or Pt-Ceria-46-atto NPs, washed and imaged afterwards. The results presented in Fig. 6 show the effect of ultrasmall platinum NPs (2–5 nm) on the surface of ceria NPs. While Pt-Ceria-46-atto NPs are mostly found distributed as filament-like structures that coincide with the mitochondrial network (Fig. 6A), internalized Ceria-47-atto NPs appear as punctate fluorescence patterns that characterize the endocytosis uptake route (Fig. 6B). The same peculiar uptake behavior of Pt-Ceria-8-atto NPs after long incubation times (Fig. 4B) was observed for Pt-Ceria-46-atto NPs. Importantly, after very short incubation periods such as 20 min, Pt-Ceria-46-atto NPs were already detected in mitochondria, but Ceria-47-atto NPs were not even detected inside the cell (data not shown). It was necessary to perform longer incubation time experiments, such as 8 h, to detect reasonable amounts of intracellular Ceria-47-atto NPs. In the present case, 83% of mitochondria are overlapped by Pt-Ceria-46-atto NPs (Fig. 6A). In contrast, only 4% of mitochondria are overlapped by Ceria-47-atto NPs (Fig. 6B). In fact, a similar result (3%) was measured for the signal of lysosomes overlapping mitochondria in Fig. 4B. Such small values for the degree of colocalization (Manders' overlap coefficient) can therefore be attributed to the proximity between vesicles and mitochondria in the cytoplasm.

Hence, platinum decoration has an enormous influence on the cellular uptake behavior of our model compounds for catalyst-derived NPs. The presence of ultrasmall platinum NPs on the surface of ceria NPs is a necessary condition for the unusual uptake mechanism under investigation.

2.5 Influence of particle size

The influence of the particle core size on the uptake behavior of catalyst-derived model NPs was investigated by comparison studies with samples synthesized under aggregation control conditions (see Fig. 2). Pt-ceria NPs of three distinct sizes were prepared: 46 nm (Pt-Ceria-46-atto), 143 nm (Pt-Ceria-143-atto), and 285 nm (Pt-Ceria-285-atto). Except for the determined differences in the particle sizes, no other remarkable differ-

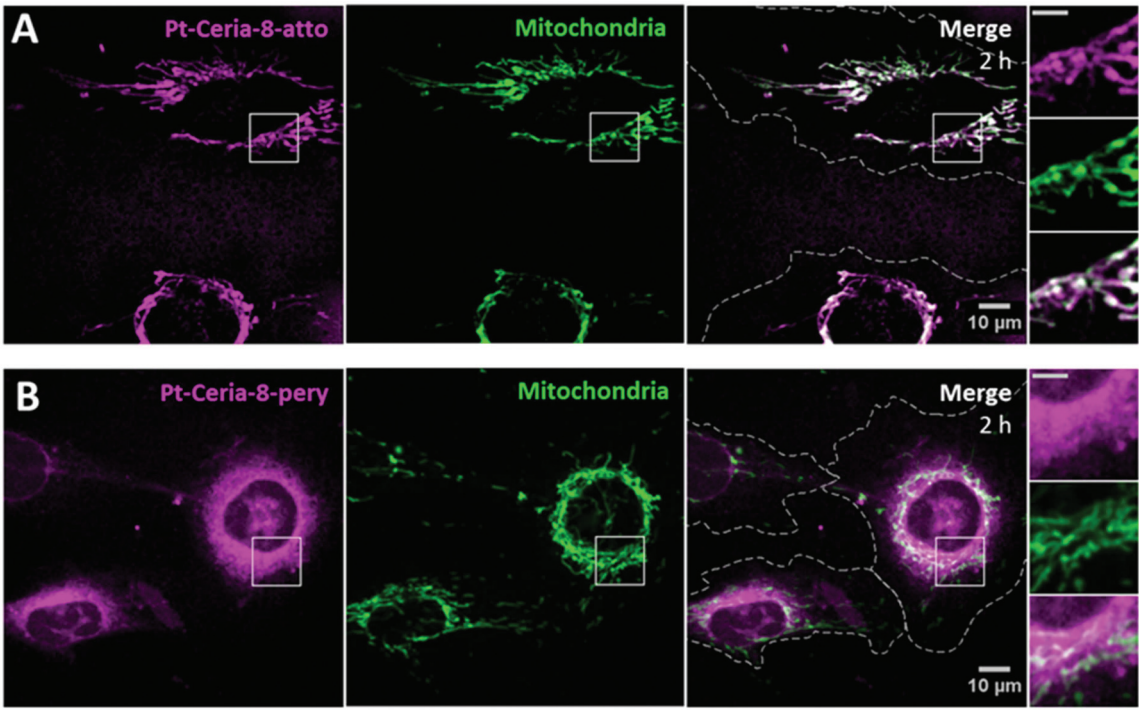

Fig. 5 Intracellular fate of 8 nm Pt-ceria NPs labeled with either Atto 647N or perylenediimide dyes. (A) HMEC-1 cells (dashed lines) were incubated with Atto 647N-labeled NPs (Pt-Ceria-8-atto) for 2 h. The expected selective association of NPs (left panel, magenta) with mitochondria (middle panel, green: MitoTracker) is evidenced in the merge image, with an overlap coefficient of 86% for the upper cell (right panel, white). Inset: boxed regions in detail. Note the typical filament-like structures of colocalizing mitochondria and NPs. Scale bar = 5 μm. (B) Parallel experiments in which HMEC-1 cells (dashed line) were incubated with perylenediimide-labeled NPs (Pt-Ceria-8-pery). A considerable amount of Pt-Ceria-8-pery NPs (left panel, magenta) can be seen inside the cells. However, in contrast to the selective mitochondrial localization of Atto 647N-labeled NPs, perylenediimide-labeled NPs are mostly diffusely distributed in the cytoplasm region. The fraction of NPs overlapping mitochondria is 46% for the cell on the right. Inset: boxed regions in detail. Note the massive presence of NPs in the cytosol and the absence of a selective accumulation in mitochondria. Scale bar = 5 μm.

ence in the physicochemical properties of the samples has been noticed (Table 1).

Cellular uptake experiments parallel to those presented in Fig. 6 were performed. The peculiar uptake behavior of the 46 nm Pt-ceria NPs is depicted in Fig. 6A. Crucially, the same trend in the uptake mechanism was not observed for larger Pt-ceria NPs. The results in Fig. 7 show that, although decorated with platinum and labeled with Atto 647N, both Pt-Ceria-143-atto and Pt-Ceria-285-atto NPs fail to associate with mitochondria. Moreover, after short incubation times, such as 20 min, no evidence of NP internalization was found (data not shown). Intracellular NPs were only detected after longer incubation times. After 8 h, a punctuate pattern of internalized Pt-Ceria-143-atto and Pt-Ceria-285-atto NPs can be visualized (Fig. 7A and B). As described previously, such a NP pattern distribution is characteristic of particle endocytosis. The fraction of mitochondria overlapped by Pt-Ceria-143-atto and Pt-Ceria-285-atto NPs was negligible (2% and 6%, respectively), and it can be attributed to the signal overlapping of NPs inside endocytic vesicles and neighboring mitochondria.

Taken together, the unusual uptake behavior observed for 46 nm Pt-ceria NPs was not observed for 143 and 285 nm Pt-ceria NPs after short or long incubation times. These results point to a remarkable particle size effect: Pt-ceria NPs smaller than ~50–100 nm escape the usual endocytic pathway and are transported directly to the cytosol by a fast uptake process; Pt-ceria NPs larger than ~150 nm, by contrast, are taken up *via* the conventional endocytosis route.

2.6 Inhibitor studies

After examining the influence of platinum decoration and particle size in the uptake behavior of Pt-ceria NPs, we investigated whether endocytosis was involved in the fast uptake mechanism observed. The most relevant and better understood endocytic pathways are clathrin-mediated endocytosis, caveolin-mediated endocytosis, macropinocytosis, and phagocytosis.[26–28] Generally, the functionality of distinct pathways is verified by live-cell imaging studies using specific labeled substrates along with endocytic inhibitors.[43–45] Transferrin glycoproteins, for example, are specifically and rapidly internalized by the clathrin-mediated pathway, while sphingolipid lactosylceramide molecules are exclusively and promptly internalized in caveolae vesicles.[36,39] Such fast uptake pathways, followed by sudden endosomal escape, would be possible mechanisms to deliver NPs directly into the cytosol. Macropinocytosis and phagocytosis are relatively slow, as they

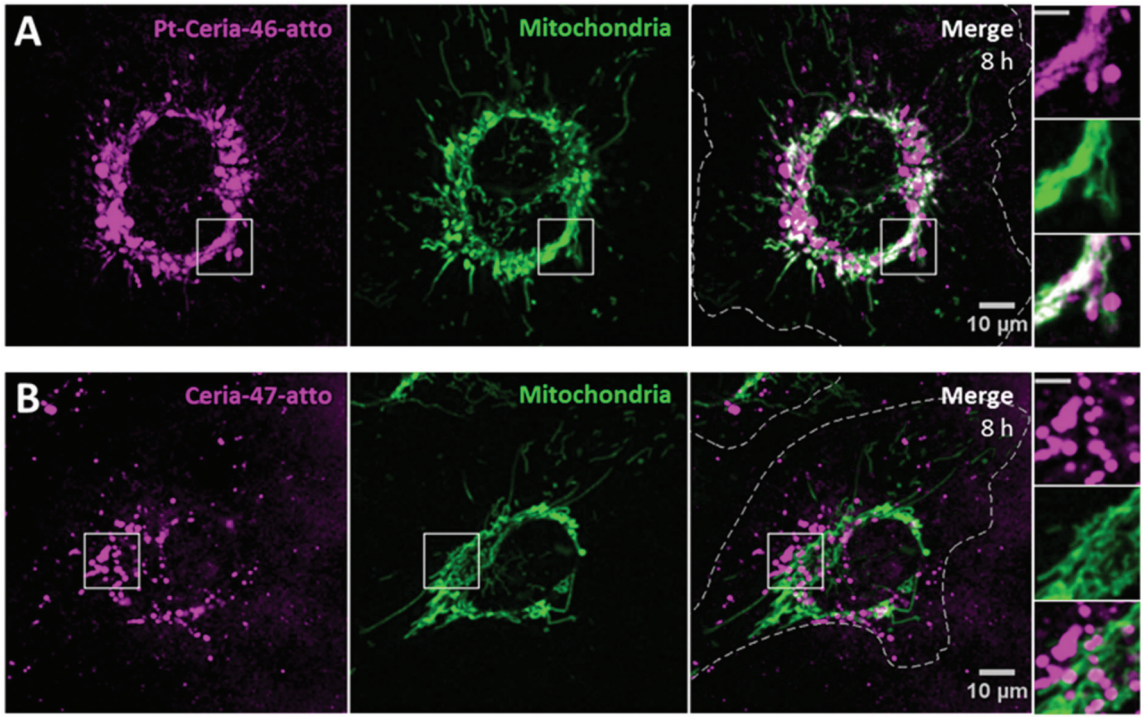

Fig. 6 Influence of platinum decoration on the cellular uptake behavior of ceria NPs. (A) Live-cell confocal images of a representative HMEC-1 cell (dashed line) incubated with Pt-Ceria-46-atto NPs (left panel, magenta) for 8 h. Cellular mitochondria (middle panel, green: MitoTracker) were stained prior to imaging. Note that NPs displaying a filament-like structure colocalize with mitochondria, while punctuate NPs do not (right panel, white pixels). Here, NPs overlap 83% of mitochondria. (B) Parallel experiments in which HMEC-1 cells (dashed lines) were incubated with Ceria-47-atto NPs (left panel, magenta). Remarkably, only the punctuate pattern of NPs, characteristic of the endocytic pathway and vesicle localization, can be observed. Moreover, no evidence of colocalization between mitochondria (middle panel, green: MitoTracker) and NPs was detected in the merge image (right panel, Manders' overlap coefficient of 4%). Inset: boxed regions in detail. Scale bars = 5 μm.

are characterized by actin-driven protrusions from the plasma membrane.[27]

In order to study the role of clathrin- and caveolin-dependent endocytosis in the uptake of small Pt-ceria NPs, we performed live-cell imaging in the presence of specific inhibitors. First, the clathrin-mediated pathway of HMEC-1 cells was completely inhibited with 15 μg mL^{-1} chlorpromazine (CP) incubated for 30 min and, after that, co-incubated transferrin was no longer internalized. In a parallel experiment, cells with the clathrin-mediated pathway completely blocked by CP were co-incubated with Pt-Ceria-46-atto NPs (100 μg mL^{-1}). A considerable amount of NPs was detected inside the cell after a short incubation time of 20 min (Fig. S2†). Once inside the cells, Pt-ceria NPs associated with mitochondria. These results indicate that the clathrin-mediated endocytosis is not involved in this uptake process. Next, we investigate the influence of caveolin-mediated endocytosis. Caveolae vesicle formation depends on the integrity of the actin network in the cell.[46] It means that actin disruption inhibits caveolin-mediated endocytosis (as well as macropinocytosis and phagocytosis).[27,47–49] For caveolin-mediated endocytosis inhibition studies, cells were incubated with cytochalasin D (CyD), a fungal toxin that promotes actin depolymerization.[49] CyD (5 μg mL^{-1}) was added to HMEC-1 cells 15 min prior to addition of Pt-ceria NPs and was present in all biological media used throughout the experiments. Inhibition of caveolin-mediated mechanism was confirmed by confocal imaging showing no internalization of sphingolipid lactosylceramide molecules (LacCer). Finally, cells with the caveolin-mediated pathway inhibited by CyD were co-incubated with Pt-Ceria-46-atto NPs (100 μg mL^{-1}). The results presented in Fig. S3† demonstrate that NPs were able to enter the cell and reach mitochondria within short incubation times, such as 20 min. These results indicate that the caveolin-mediated endocytosis as well as other actin-dependent mechanisms are not involved in the uptake process of small Pt-ceria NPs.

It is reported in the literature that cell membrane penetration by ultrasmall NPs (*e.g.* 6–10 nm) is an energy-independent process. Therefore, NP internalization occurs not only at 37 °C, but also with cells maintained at 4 °C.[32,50] However, these studies also show that the amount of internalized NPs is typically drastically reduced at 4 °C. The reduced number of internalized NPs is probably influenced by changes in the mechanical properties of lipid bilayers at low temperatures.[51,52] To investigate the uptake behavior of small Pt-ceria NPs at 4 °C we incubated HMEC-1 cells with Pt-Ceria-46-atto (100 μg mL^{-1}) on ice for 30 min. In our results, no internalization of Pt-ceria NPs at 4 °C was detected (data not shown).

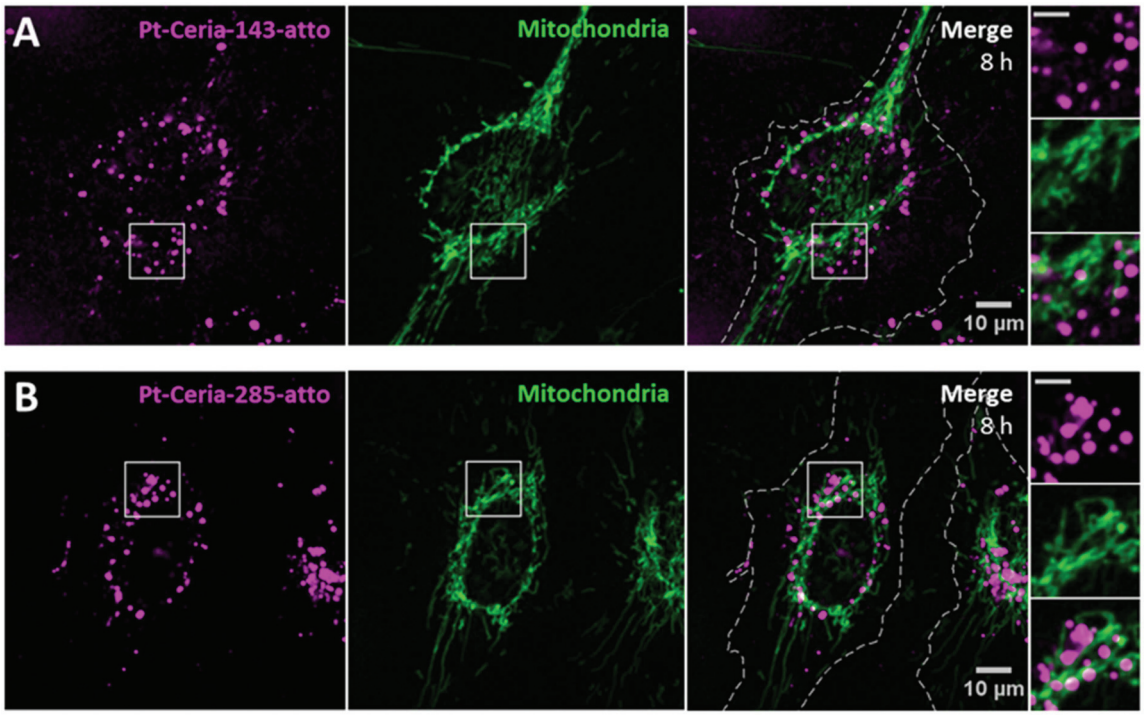

Fig. 7 Influence of particle size on the cellular uptake behavior of Pt-ceria NPs. Live-cell confocal images of HMEC-1 cells (dashed lines) incubated with either (A) Pt-Ceria-143-atto NPs or (B) Pt-Ceria-285-atto NPs for 8 h. Similar results were achieved with both samples, and a punctuate pattern typical of particle endocytosis was observed (left panels, magenta). In addition, the absence of NP accumulation in mitochondria (middle panels, green: MitoTracker) can be noticed in the merge images (right panels). The fraction of Pt-Ceria-143-atto and Pt-Ceria-285-atto NPs overlapping mitochondria is only 2% and 6%, respectively. Such small values can be attributed to the signal of NPs in endosomes overlapping nearby mitochondria. Insets: boxed regions in detail. Note the punctuate pattern of NPs distributed in the vicinity, but not in mitochondria. Scale bars = 5 μm.

Yet, upon warming of cells back to 37 °C, fast internalization of NPs occurred. The observed inhibition of Pt-ceria NP uptake at 4 °C may have been influenced by the core sizes of our particles (see Table 1), which are significantly larger than the abovementioned ultrasmall NPs. We hypothesize that Pt-ceria NPs are not able to translocate membranes at 4 °C due to changes in the elastic properties of cell membranes at low temperatures.

2.7 Protein corona

NPs are normally covered by a protein corona as they interact with proteins present in biological media. The protein corona can largely define the biological identity of a given NP, and it can therefore influence the effect of this NP on a cellular level.[53] The results described so far have all been obtained with cell media supplemented with 10% fetal bovine serum (FBS). With the purpose of verifying if the presence of serum proteins in cell culture medium plays a decisive role in the interaction between Pt-ceria NPs and cells, we incubated HMEC-1 cells with Pt-Ceria-46-atto NPs (100 μg mL^{-1}) in a cell medium formulation free of FBS. Interestingly, the outcomes were not distinct from those measured in the presence of serum proteins, and NPs were found inside the cells and associated with mitochondria (Fig. S4†). Thus, the presence of serum proteins (in solution or forming a protein corona adsorbed to the NP surface) does not influence the unusual uptake behavior observed for small Pt-ceria NPs. These results indicate an uptake mechanism driven by the physicochemical properties of the bare surface of NPs. In addition, these results are in line with the cell membrane penetration by ultrasmall gold NPs in both serum-free and serum-containing cell medium.[32]

2.8 Cell membrane integrity

So far, all results point toward cell membrane penetration by small Pt-ceria NPs. Cell membrane penetration by NPs can cause the disruption of the plasma membrane and induce cytotoxic effects.[54] In addition, the leakage of ions or molecules into or out of the cell through permanent holes on the membrane can lead to cell death.[32] To verify whether Pt-ceria NPs cause permanent holes or any other damage to the plasma membrane integrity, we performed calcein leakage in and out assays.

First, we tested if the direct translocation of Pt-ceria NPs through the membrane was accompanied by the leakage in (or penetration) of co-incubated calcein. The fluorescent dye calcein cannot penetrate an intact cell membrane directly, but is normally internalized by endocytosis and remains enclosed by intracellular vesicles. However, if the membrane is disrupted, calcein can penetrate the cell and a diffuse pattern is

observed throughout the cytosol. Scoring the percentage of cells without the cytosolic calcein distribution is a convenient way to access the viability of cells after exposure to external agents. Cell membrane damage caused by external agents is typically characterized by the majority of cells exhibiting cytosolic calcein. For example, Verma *et al.*[32] showed that cationic gold NPs (coated with 11-mercaptoundecane-tetramethylammonium chloride) which are able to disrupt membranes, led to cytosolic calcein distribution in ~50% of the dendritic cells, while in the control samples not treated with gold NPs, 95% of the cells were found without calcein cytosolic distribution.

We co-incubated HMEC-1 cells with cell medium containing 0.1 mg mL^{-1} calcein and 100 μg mL^{-1} Pt-Ceria-46-atto NPs for 3 h. After this, cells were washed and imaged live. The percentage of cells without calcein distribution was above 97%. Besides, no significant difference in the viability of untreated and NP treated cells was found (Fig. S5†).

Next, we performed complementary studies on the particle-induced leakage out (or release) of previously internalized cytosolic calcein. The cell-permeant and nonfluorescent calcein-AM dye can access the cytosolic compartment of living cells and, once there, it is converted to the fluorescent calcein by intracellular esterases and remains trapped in the cytosol. In our experiments, HMEC-1 cells were preincubated with 5 μM calcein-AM for 45 min. Calcein-loaded cells were washed with cell medium and incubated with 100 μg mL^{-1} Pt-Ceria-46-atto NPs for 0.5 and 3 h. After the respective incubation periods, cells were washed again and imaged live. The mean fluorescence intensity of cytosolic calcein was measured in untreated cells and in cells treated with Pt-ceria NPs (Fig. S6†). The data show that no leakage out of pre-loaded cytosolic calcein was induced by the uptake of NPs. Moreover, no significant difference between untreated and NP treated cells was detected. These results are in line with the previous findings on the leakage in of calcein (Fig. S5†). Altogether, calcein leakage in and out assays offer supporting evidence that small Pt-ceria NPs can access the cytosol without causing noticeable membrane disruption.

2.9 Impact of ceria and Pt-ceria NPs on the cellular ATP level

In order to further investigate if small Pt-ceria NPs can have an impact on cellular viability, we measured and compared the particle-induced cytotoxicity of (non-labeled) Ceria-47, Pt-Ceria-46, and Pt-Ceria-143 NPs. HMEC-1 cells were incubated at two distinct concentrations: 10 μg mL^{-1} and 100 μg mL^{-1}. After specific incubation periods of 3, 24, 48 and 72 h, the relative adenosine triphosphate (rATP) content was analyzed to assess the metabolic impact of NPs on cells. One hundred percent rATP content represents the cellular viability of untreated cells. As presented in Fig. 8, the rATP contents of cells treated with Pt-Ceria-46 NPs do not significantly differ from the rATP values of cells incubated with either Ceria-47 or Pt-Ceria-143 NPs. In addition, there is no significant difference in the cytotoxicity of non-labeled and Atto 647N labeled 46 nm Pt-ceria NPs (100 μg mL^{-1}; Fig. 8B). This means that platinum decoration and the unconventional uptake mechanism of Pt-Ceria-46-atto NPs do not induce a different nanotoxicity under

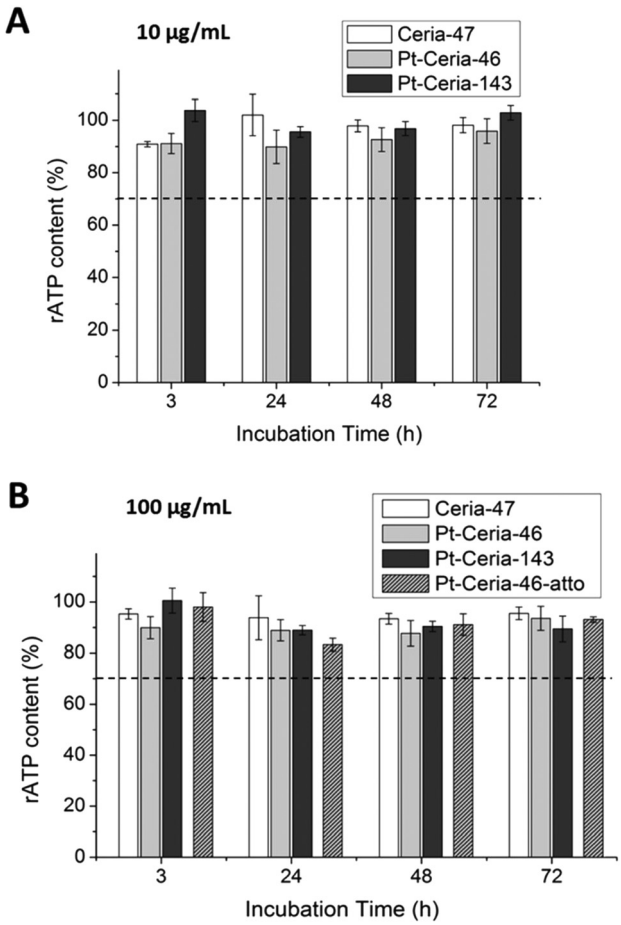

Fig. 8 Cellular viability of cells treated with ceria and Pt-ceria NPs. HMEC-1 cells were exposed to either (A) 10 μg mL^{-1} or (B) 100 μg mL^{-1} of distinct NP samples: Ceria-47 NPs (white bars), Pt-Ceria-46 NPs (light gray bars), Pt-Ceria-143 NPs (dark gray bars), and Pt-Ceria-46-atto NPs (light gray striped bars). The incubation time extended from 3 to 72 h. Within this time, no significant difference ($p < 0.01$) was detected in the relative adenosine triphosphate (rATP) content of cells exposed to any NP type (in comparison to the other NP types). In addition, the rATP content measured was always above the cytotoxicity threshold of 70% (dashed line, cytotoxicity according to DIN EN ISO 109935:2009-10). This means that the metabolic impact induced by all these NP types on HMEC-1 cells was quite low. Histograms represent the mean ± standard error from three independent experiments.

the investigated conditions. Moreover, the rATP values were found to be above the cytotoxic threshold of 70% (dashed line) under all investigated conditions. This is a clear indication that ceria and Pt-ceria NPs are well tolerated by HMEC-1 cells in short-term exposure experiments (3–72 h).

2.10 Cell-penetrating Pt-ceria NPs

As described in the literature, cell-penetrating peptides,[29] quantum dots,[30] and ultrasmall noble metal NPs (<~10 nm), such as gold[31–35] and platinum,[36,37] can escape the endocytic pathway and translocate the plasma membrane into the cytosol. This unconventional pathway is characterized by fast and efficient cellular uptake, no perceptible cell membrane

disruption and low cytotoxic effects.[31] This description almost perfectly matches our findings on the unusual fast uptake mechanism and cytosolic delivery of small Pt-ceria NPs. The exception is the presence of a relatively large ceria NP core.

So as to test the generality of our results, we prepared 8 nm ceria NPs decorated with other noble metals; namely, rhodium and palladium. In addition, we synthesized platinum-decorated 50–80 nm mesoporous silica NPs. Preliminary results indicate that in all cases the same trend, with cell membrane penetration and mitochondrial targeting by Atto 647N-labeled NPs was achieved (data not shown). Moreover, we investigated if the uptake trend observed for small Pt-ceria NPs is cell-type dependent. Human cervical cancer cells (HeLa) were incubated with Pt-Ceria-8-atto NPs, and the same unusual uptake behavior observed before was observed for HeLa cells (Fig. S7†).

In order to gain more information regarding the cell membrane penetration and mitochondrial association of Pt-ceria NPs we performed transmission electron microscopy (TEM) of cells. First, HeLa cells were incubated with non-labeled (Pt-Ceria-46) as well as Atto 647N-labeled particles (Pt-Ceria-46-atto) for 2 h. Subsequently, specimens were fixed, dehydrated, infiltrated, embedded, cured, cut in thin sections of 80–90 nm, mounted, stained, and finally examined by TEM (for details see section 3.4). Remarkably, the results presented in Fig. 9A are in line with the hypothesis of cell membrane penetration of small, individual Pt-ceria NPs as well as conventional endocytosis of particle aggregates. In addition, the micrograph shown in Fig. 9B suggests the accumulation of targeted NPs (Pt-Ceria-46-atto) on the outer membrane of mitochondria. Yet, the production of the TEM micrographs of cells relies on standard but quite elaborated fixation, staining, embedding and ultrathin sectioning protocols that may create artifacts. These TEM images should therefore be interpreted with care and regarded as an indication of the presence of Pt-ceria NPs in the respective cellular compartments, as thoroughly shown by the live-cell imaging results presented in this work.

On the basis of our findings and the literature, we propose the following uptake mechanism for small Pt-ceria NPs: as one NP diffuses and approaches a cell, the ultrasmall platinum NPs on its surface generate multiple transient nanoscale holes. These holes combine and allow the membrane penetration of the NP up to a core size of ~50–100 nm. After the passage of the particle, the membrane rapidly reseals itself. Once inside the cells, the diffusing NP will come into contact with cell organelles and, in the case of Pt-ceria NPs labeled with Atto 647N, will attach to mitochondria owing to the lipophilic cationic moieties of this dye. Fig. 10 illustrates graphically the cell membrane penetration and mitochondrial targeting by a 50 nm Pt-ceria NP.

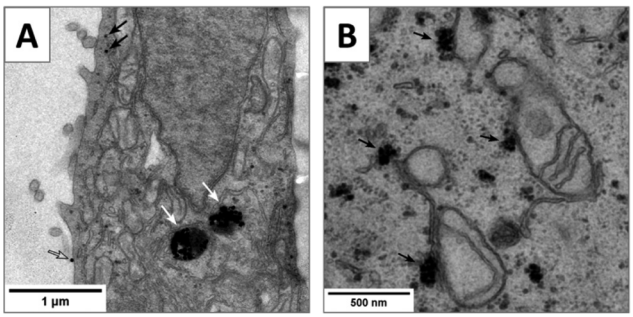

Fig. 9 TEM images of Pt-ceria NPs of 46 nm internalized by HeLa cells. Electron micrographs of thin transverse sections (80–90 nm) (A) indicating the presence of non-labeled Pt-Ceria-46 in the cytosol (black arrows), in endosomes (white arrows), and on the plasma membrane (open arrow) and (B) suggesting the accumulation of Pt-Ceria-46-atto on the outer surface of mitochondria (black arrows).

3. Experimental details

3.1 Synthesis and characterization of ceria and Pt-ceria NPs

The influence of the reaction parameters on the synthetic procedures is discussed by Herrmann *et al.*,[18] and experimental

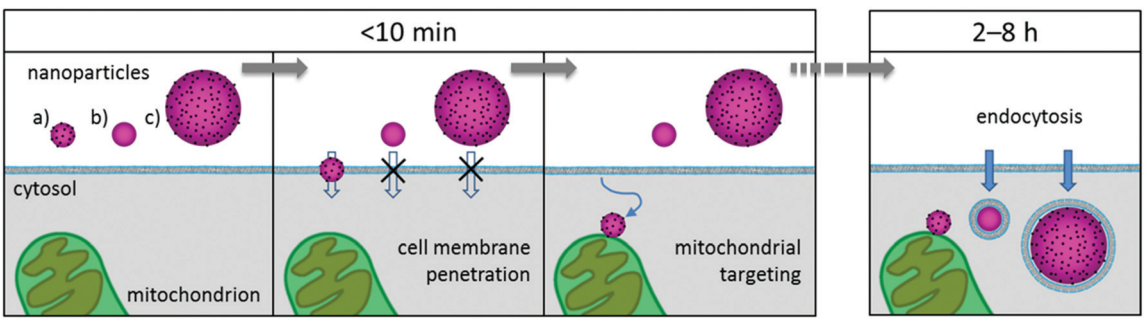

Fig. 10 Cell membrane penetration and mitochondrial targeting by Pt-ceria NPs. Within a few minutes of incubation time, three mitochondria-targeted NPs approach a cell: (a) 50 nm Pt-ceria NP, (b) 50 nm ceria NP, and (c) 150 nm Pt-ceria NP. In the case of particle (a), ultrasmall platinum NPs decorating its surface induce nanoscale holes on the cell membrane, and the NP directly translocates from the extracellular environment into the cytosol. Particle (b) is not able to translocate the membrane because it is free of ultrasmall platinum NPs on its surface. Particle (c) is too large to pass through eventually induced holes. After translocation, particle (a) diffuses freely in the cytosol and the membrane reseals. Next, the diffusing NP reaches and attaches to a mitochondrion. After a few hours, the particles (b) and (c) are internalized by the conventional endocytic pathway and remain trapped in vesicles.

details are given here. Deionized water and dry ethanol (Emsure quality, Merck) were used for all syntheses.

Ceria NPs. The procedure was adapted from that used by Yu *et al.*[55] $Ce(NO_3)_3{\cdot}6H_2O$ (2.0 mmol, 870 mg) was dissolved in a mixture of 18 mL of ethanol and 1 mL of water. The solution was heated in a round bottom flask (not covered, needs contact with air) to 70 °C under stirring. Ammonia (25%) was added in one portion (1.0 mL). A thick precipitate formed which became a slightly yellowish suspension after stirring for 2 hours. Care had to be taken as the solvent did not evaporate during this time. After cooling to room temperature, stirring was continued for *ca.* 15 h. The resulting particles were separated by centrifugation (9500*g*, 15 min), and washed three times with water (12 mL) and three times with ethanol (12 mL), each step consisting of redispersion by ultrasound treatment in the appropriate solvent and centrifugation under the same conditions as before. The product, ceria NPs of 8 nm average diameter, was stored in ethanol.

Controlled aggregation of ceria NPs. The procedure was adapted from that described by Wang *et al.*[56] A 4 mL screw cap glass vial with a Teflon gasket (Wheaton) was charged with $Ce(NO_3)_3{\cdot}6H_2O$ (99%, Sigma-Aldrich) and poly(vinylpyrrolidone) (PVP), average M_w 55 000 (Sigma-Aldrich), dissolved in a mixture of water and ethanol. The vial was tightly closed and stirred at an appropriate oil bath temperature for the time indicated. After cooling to room temperature the nanoparticles were isolated by centrifugation and washed with water (3 times, 2 mL) and ethanol (3 times, 2 mL) as described before. The amounts of the starting material and the reaction conditions are given in Table 2 (compare Table 1).

Platinum decoration of ceria NPs. To a ceria nanoparticle dispersion in ethanol (20 mg in 0.5 mL) in a 4 mL screw cap glass vial with a Teflon gasket (Wheaton) the precursor K_2PtCl_4, dissolved in 3 mL of water, was added. The vial was closed and the reaction mixture was stirred at 70 °C (oil bath temperature) for 17 h. After cooling, solid KBH_4 (*ca.* 5 mg) was added (caution: foaming) and stirring continued for 1 h at room temperature. The particles were isolated by the centrifugation procedure and washed with water (3 times, 2 mL) and ethanol (3 times, 2 mL) as described before. The product was stored in ethanol.

Labeling with fluorescent dyes. The perylenediimide marker (MPD-APS) was prepared as described by Blechinger *et al.*[57] The Atto 647N marker (Atto 647N-APS) was obtained from a commercial Atto 647N NHS ester (Sigma-Aldrich) by reaction with 3-(triethoxysilyl)propylamine (APS). Thus, the NHS ester (0.85 mg, 1 μmol) in 80 μL of *N*,*N*-dimethylformamide was added to a solution of APS (1 μmol mL^{-1}) in ethanol (1.5 mL) and stirred for 5 h at room temperature. Thin layer chromatography (silica, chloroform/ethanol 1 : 1) showed complete conversion (NHS ester: retardation factor R_f 0.81, Atto 647N-APS: R_f 0.87). The solution was stored at 5 °C in the dark and used without further purification for nanoparticle labeling. To the nanoparticle dispersion (20 mg) in ethanol (1.5 mL) was added 100 μL of the Atto 647N-APS solution, or 50 μL of MPD-APS (15 μmol mL^{-1} in chloroform), respectively, and the mixture was stirred in a closed screw cap vial (Wheaton) for 5 h at 120 °C (oil bath temperature); for MPD-APS, 140 °C was applied. Stirring was continued for 20 h at room temperature. The labeled particles were isolated by centrifugation and purified by redispersion in ethanol and centrifugation (4 times, 2 mL) as described before. The particles were stored in ethanol in the dark.

Transmission electron microscopy (TEM) and energy-dispersive X-ray (EDX) spectroscopy. TEM and EDX images were obtained with a JEM 2100 F (JEOL) instrument. Nanoparticle dispersions were diluted with ethanol and applied onto carbon-coated copper grids (Formvar coal-film on a 200 mesh net; Plano GmbH). Particle sizes were determined from TEM images by digital image analysis using the ImageJ software.[58]

Particle size distribution and zeta potential determinations. Dynamic light scattering (DLS) measurements were employed to determine the intensity weighted mean hydrodynamic diameter of the ceria and Pt-ceria NPs. Investigations on the electrophoretic mobility of the nanoparticles were carried out to determine the zeta potential. Both studies were conducted with Zetasizer Nano equipment (Malvern Instruments) on colloidal NP suspensions in either ethanol or in cell medium supplemented with 10% FBS (incubation time of 30–40 min).

3.2 Incubation of cells with NPs

Cell culture. HMEC-1 cells (Centers for Disease Control and Prevention, USA) were grown in Gibco MCDB 131 medium supplemented with 10% fetal bovine serum (FBS), 1% GlutaMAX-I (100X), 10 ng mL^{-1} human epidermal growth factor (all purchased from Life Technologies), and 1 μg mL^{-1} hydrocortisone (Sigma-Aldrich). HeLa cells were grown in Gibco Dulbecco's modified Eagle's medium (DMEM; Life Technologies, Germany) supplemented with 10% FBS. Cells were maintained at 37 °C under a humidified atmosphere containing 5% CO_2.

Redispersion of NPs in cell medium. Dispersions of ceria NPs and Pt-ceria NPs were prepared in the same cell medium used for cell growth according to the following procedure: first, the stock dispersion of NPs (in ethanol) was vortexed for 10 s, treated with an ultrasonic bath for 10 min, and vortexed again for 10 s; next, a small aliquot (up to a few μL) of the

Table 2 Starting material and reaction conditions

Sample	$Ce(NO_3)_3{\cdot}6H_2O$ [mg]	PVP [mg]	Ethanol [mL]	Water [mL]	Temperature [°C]	Time [h]
Ceria-47	56	216	1.5	0.5	140	6
Ceria-143	108	56	1.5	0.5	130	20
Ceria-285	108	56	0.67	1.34	140	13

ethanolic suspension of NPs was added into a microcentrifuge tube (1.5–2 mL; Eppendorf); ethanol was then left to evaporate completely under a laminar flow or under a gentle stream of N_2; after complete evaporation of ethanol, the tube with the dried NPs was closed and reserved for up to 6 hours; shortly before addition to cells, a given volume of cell medium (so as to reach the desired NP concentration) was added to the dried NPs in the tube; finally, particles were immediately dispersed in the medium by sonication, warmed up to 37 °C, and added to cells.

Uptake experiments. For live-cell imaging experiments, cells were seeded 24 h before imaging in Lab-Tek II 8-well chamber slides (Thermo Fisher Scientific Inc.) in a density of 1.2×10^4 cells per cm^2. HMEC-1 cells were incubated with NPs at 37 °C under a humidified atmosphere containing 5% CO_2.

Uptake kinetics, intracellular fate, and mitochondrial targeting. Cell plasma membranes were stained with a wheat germ agglutinin Alexa Fluor 488 conjugate (WGA 488, 10 μg mL^{-1} in cell medium for 1 min) or with CellMask Orange (0.05% (v/v) in cell medium for 1–2 min). Mitochondria were stained with MitoTracker Green FM (100 nM in cell medium for 15–30 min) or with MitoTracker Red CMXRos (60 nM in cell medium for 10 min). Cellular lysosomes were stained with LysoTracker Red (150 nM in cell medium for 30 min; all organelle-specific stains were purchased from Life Technologies). In all cases, after the indicated incubation times, the respective staining solution was removed and cells were washed twice with warm cell medium. Cell medium containing the NPs was then added to cells. Cells were imaged live as described below.

Inhibitor studies. To investigate if endocytosis was involved in the fast uptake behavior of Pt-ceria NPs, inhibition studies were conducted. To ensure a complete inhibition of the clathrin-dependent uptake pathway, HMEC-1 cells were incubated with 15 μg mL^{-1} chlorpromazine (Sigma-Aldrich) for 30 min prior to addition of further substrates. To probe the clathrin-mediated endocytosis, inhibited cells were then co-incubated with transferrin (20 μg mL^{-1}; Life Technologies) or Pt-ceria NPs (100 μg mL^{-1}) for 20 min. To visualize the uptake, the cell membrane was stained with CellMask Orange (as described above, but in cell medium containing 15 μg mL^{-1} chlorpromazine). Live-cell imaging was performed in the presence of the inhibitor, except for the uptake of transferrin in the absence of chlorpromazine, as shown in Fig. S2A.† The caveolin-dependent mechanism was efficiently inhibited with 5 μg mL^{-1} cytochalasin D (CyD; Sigma-Aldrich). HMEC-1 cells were incubated with CyD for 15 min prior to addition of further substrates. To investigate the caveolin-mediated pathway, inhibited cells were co-incubated with 0.5 μM sphingolipid lactosylceramide (LacCer; Life Technologies) or Pt-ceria NPs (100 μg mL^{-1}) for 20 min. All experiments were performed in the presence of the inhibitor, except for the uptake of LacCer in the absence of CyD (Fig. S3A†).

Cell membrane integrity. For calcein leakage in (or penetration) assay, HMEC-1 cells were co-incubated with cell medium containing 0.1 mg mL^{-1} calcein (Life Technologies) and 100 μg mL^{-1} of Pt-ceria NPs for 3 h. After the incubation time, cell plasma membranes were stained with CellMask Orange (see above) and imaged as described below. For calcein leakage out (or release) assay, HMEC-1 cells were preincubated with 5 μM calcein-AM (Life Technologies) for 45 min. Calcein-loaded cells were then washed with cell medium and incubated with 100 μg mL^{-1} of Pt-ceria NPs for 0.5 and 3 h. After the respective incubation periods, cells were washed again and imaged live.

Colocalization studies. Manders' overlap coefficients were determined by using the ImageJ plugin JACoP developed by Bolte and Cordelieres.[38]

Cytotoxicity studies. For cytotoxicity evaluation (see below), 1.2×10^4 HMEC-1 cells per cm^2 were seeded in 96-well cell culture plates. 24 h after seeding, cells were exposed to either ceria NPs or Pt-ceria NPs dispersed in cell medium (as described above) at 37 °C under a humidified atmosphere containing 5% CO_2.

3.3 Live-cell imaging

Spinning disk confocal microscopy was performed on a setup based on the Zeiss Cell Observer SD equipped with a Zeiss Plan Apochromat 63×/1.40 Oil/DIC objective. Samples were maintained at 37 °C under a 5% CO_2 atmosphere during imaging and were illuminated with laser light alternating between 488 nm (exciting WGA 488, MitoTracker Green, perylenediimide, calcein, or LacCer), 561 nm (exciting CellMask Orange, MitoTracker Red, or LysoTracker Red), and 639 nm (exciting Atto 647N). The emission signal was split by using a dichroic mirror at 560 nm (for dual-color detection upon excitation with 488 or 639 nm light) or at 660 nm (for three-color detection upon excitation with 488, 561 or 639 nm light). Separate images for each fluorescence channel were sequentially acquired using two separate electron multiplier charge-coupled device cameras (Evolve 512; Photometrics). The bandpass detection filters of the first camera, installed in an automatic revolving filter wheel, were 525/50 nm (WGA 488/MitoTracker Green/perylenediimide/calcein/LacCer channel) and 629/62 nm (CellMask Orange/MitoTracker Red/LysoTracker Red channel). The bandpass filter used for the second camera was 690/50 nm (Atto 647N channel). Exposure times were set to 100–500 ms. The *Z*-stacks of single cells were imaged with an interslice distance of 250 nm.

3.4 Characterization of nanoparticle uptake using TEM

TEM specimen preparation (fixation, dehydration, infiltration, embedding, curing, thin sectioning, mounting and staining) of cells incubated with Pt-ceria NPs was performed using standard procedures as follows: HeLa cells were cultivated as described above and seeded onto Falcon cell culture inserts (high pore density translucent PET membranes with a pore size of 0.4 μm; Corning) placed into a companion Falcon 24-well culture plate. The lower compartments of the wells were filled with prewarmed culture medium (700 μL) and cells were seeded onto the inserts at a density of 6.6×10^4 cells per cm^2 (200 μL). After 24 h incubation with cell medium, dispersions of the Pt-ceria NPs prepared as described before (see section

3.2) were added to the cells. HeLa cells were incubated with NPs (100 μg mL^{-1}) for 2 h at 37 °C under a humidified atmosphere containing 5% CO_2. Cells were fixed overnight with a half strength Karnovsky's fixative (2.5% paraformaldehyde, 3.0% glutaraldehyde, and 0.06% calcium chloride in 0.1 M cacodylate buffer) at 4 °C. Here and in the following steps using the cell culture inserts, 200 μL of the working solution were added to the top and 700 μL to the bottom chamber. After fixation cells were washed (3 times, 15 min) with 0.1 M cacodylate buffer (Morphisto GmbH) and then placed for 6 h with 0.1 M cacodylate buffer at 4 °C. Next, cells were post-fixed for 2 h at 4 °C with a solution containing 1% osmium tetroxide (Sigma Aldrich) and 1.5% potassium ferrocyanide (Carl Roth) in 0.1 M cacodylate buffer (freshly prepared using one part of a 2% osmium tetroxide solution and another part of a 3% potassium ferrocyanide solution). Cells were washed with 0.1 M cacodylate buffer (3 times, 15 min and then overnight at 4 °C). Next day cells were washed with PBS (15 min) and the membranes containing the cells were removed from the inserts using a sharp razor blade. The membranes were then placed into individual microcentrifuge tubes (1.5 mL; Eppendorf) and dehydration of the cells was performed under slight agitation (300 rpm; Thermomixer Comfort, Eppendorf) in a graded ethanol series at RT (1 mL; 30%, 50%, 70%, 20 min each; 95%, 30 min; and 100% 3 times, 30 min). For embedding we used the Poly/Bed 812 Embedding Kit (Polyscience). Prior to embedding cells were infiltrated at RT in four steps with a propylene oxide/embedding mixture (1 mL; twice 1 : 0, 15 min; then 2 : 1, 1 : 1 and 0 : 1, 1 h each). Infiltration was performed under slight agitation (300 rpm, Thermomixer Comfort; Eppendorf). The membranes were transferred from the tubes (containing 100% embedding medium) to embedding molds (Plano GmbH, cat. no. G369N). Molds containing the membranes were filled with embedding medium and cured at 60 °C for 30 h. Afterwards, ultrathin sections of 80–90 nm thickness were cut using a ultramicrotome (Leica-Reichert Ultracut E), mounted onto copper grids (Formvar-carbon 300 mesh; Ted Pella, Inc.) and stained with uranyl acetate (8% for 10 min) and Reynold's lead citrate solution (2.2% for 3 min). Finally, specimen sections were examined on a transmission electron microscope (JEM 1011, JEOL).

3.5 Cytotoxicity studies

To assess the relative cellular ATP content, cells were seeded as described above. The culture medium was then replaced with a fresh one containing either 10 μg mL^{-1} or 100 μg mL^{-1} of NPs. After defined incubation times (3, 24, 48, and 72 h), cells were washed with Hank's balanced salt solution. Next, CellTiter-Glo Luminescent Cell Viability Assay (Promega GmbH) was used according to manufacturer's instructions. The relative ATP content of the cells was calculated from the measured luminescence (LUMIStar Galaxy; BMG LABTECH GmbH) and expressed as the relative value compared to untreated control cells. To interpret the impact of the ceria NPs as well as Pt-ceria NPs on endothelial cells, the threshold for cytotoxicity according to DIN EN ISO 10993-5:2009-10 was considered.

3.6 Statistical analysis

For statistical analysis, the unpaired Student's *t*-test was used. The values were expressed as the mean ± standard error. The results were considered as statistically different at $p < 0.05$ and highly statistically different at $p < 0.01$.

4. Conclusions

In summary, platinum-decorated ceria NPs that resemble catalyst-derived particles can escape the traditional endocytosis uptake pathway and perform a rapid and direct translocation through the cell membrane. Interestingly, similar ceria NPs free of platinum do not translocate through the membrane, but are internalized by endocytosis. In addition, the particle size is a crucial parameter – only Pt-ceria NPs smaller than ~50–100 nm are able to perform cell membrane penetration. If suitably targeted, these NPs are able to selectively attach to cellular organelles like mitochondria. Mitochondrial targeting was achieved at first by chance with Atto 647N, a fluorescent dye with high affinity to this cell organelle.

The results presented in this work make distinguished contributions to the fields of nanotoxicology and nanomedicine. As regards nanotoxicology, although the uptake mechanism proposed involves the fast translocation of Pt-ceria NPs into the cytosol, our findings suggest that the short-term nanotoxicology of high doses of Pt-ceria NPs (within 72 h, 100 μg mL^{-1}) is rather low. However, long-term effects of continuous exposure to much lower doses, as in human exposure to air pollution, remain to be investigated. With respect to nanomedicine, Pt-ceria NPs (and conceivably other noble-metal decorated NPs) are fascinating materials that can rapidly and efficiently enter cells and reach intracellular organelles, such as mitochondria. In this way they represent an interesting particle type with high potential to become important platforms for intracellular-targeted drug and gene delivery.

Acknowledgements

This work was supported by the Deutsche Forschungsgemeinschaft DFG, project SPP1313, as well as by the Center for NanoScience (CeNS) and the excellence clusters Nanosystems Initiative Munich (NIM) and Center for Integrated Protein Science Munich (CIPSM). The technical assistance of Jaroslava Obel is acknowledged. We thank Thomas Bein (University of Munich, Germany) for providing the instrument for DLS and zeta potential measurements.

Notes and references

1 United States Environmental Protection Agency (EPA). Six Common Air Pollutants, http://www.epa.gov/criteria-air-pollutants (accessed May 2016).

2 R. D. Brook, S. Rajagopalan, C. A. Pope 3rd, J. R. Brook, A. Bhatnagar, A. V. Diez-Roux, F. Holguin, Y. Hong, R. V. Luepker, M. A. Mittleman, A. Peters, D. Siscovick, S. C. Smith Jr., L. Whitsel and J. D. Kaufman, *Circulation*, 2010, **121**, 2331–2378.
3 C. Buzea, I. Pacheco and K. Robbie, *Biointerphases*, 2007, **2**, MR17–MR71.
4 K. Donaldson, R. Duffin, J. P. Langrish, M. R. Miller, N. L. Mills, C. A. Poland, J. Raftis, A. Shah, C. A. Shaw and D. E. Newby, *Nanomedicine*, 2013, **8**, 403–423.
5 A. Zanobetti, F. Dominici, Y. Wang and J. Schwartz, *Environ. Health*, 2014, **13**, 38.
6 D. Loomis, Y. Grosse, B. Lauby-Secretan, F. E. Ghissassi, V. Bouvard, L. Benbrahim-Tallaa, N. Guha, R. Baan, H. Mattock and K. Straif, *Lancet Oncol.*, 2013, **14**, 1262–1263.
7 International Agency for Research on Cancer (IARC). World Health Organization (WHO). Press Release No. 221 (17 October 2013). IARC: Outdoor air pollution a leading environmental cause of cancer deaths, http://www.iarc.fr/en/media-centre/iarcnews/pdf/pr221_E.pdf (accessed May 2016).
8 P. Kumar, A. Robins, S. Vardoulakis and R. Britter, *Atmos. Environ.*, 2010, **44**, 5035–5052.
9 P. Kumar, L. Morawska, W. Birmili, P. Paasonen, M. Hu, M. Kulmala, R. M. Harrison, L. Norford and R. Britter, *Environ. Int.*, 2014, **66**, 1–10.
10 F. Alt, A. Bambauer, K. Hoppstock, B. Mergler and G. Tölg, *Fresenius' J. Anal. Chem.*, 1993, **346**, 693–696.
11 K. H. Ek, G. M. Morrison and S. Rauch, *Sci. Total Environ.*, 2004, **334–335**, 21–38.
12 B. Gómez, M. Gómez, J. L. Sanchez, R. Fernández and M. A. Palacios, *Sci. Total Environ.*, 2001, **269**, 131–144.
13 E. Helmers, *Chemosphere*, 1996, **33**, 405–419.
14 M. A. Palacios, M. M. Gómez, M. Moldovan, G. Morrison, S. Rauch, C. McLeod, R. Ma, J. Laserna, P. Lucena, S. Caroli, A. Alimonti, F. Petrucci, B. Bocca, P. Schramel, S. Lustig, M. Zischka, U. Wass, B. Stenbom, M. Luna, J. C. Saenz, J. Santamaría and J. M. Torrens, *Sci. Total Environ.*, 2000, **257**, 1–15.
15 L. Qi, M.-F. Zhou, Z. Zhao, J. Hu and Y. Huang, *Environ. Earth Sci.*, 2011, **64**, 1683–1692.
16 S. Rauch, H. F. Hemond, C. Barbante, M. Owari, G. M. Morrison, B. Peucker-Ehrenbrink and U. Wass, *Environ. Sci. Technol.*, 2005, **39**, 8156–8162.
17 H. Wichmann, G. A. K. Anquandah, C. Schmidt, D. Zachmann and M. A. Bahadir, *Sci. Total Environ.*, 2007, **388**, 121–127.
18 R. Herrmann, M. Rennhak and A. Reller, *Beilstein J. Nanotechnol.*, 2014, **5**, 2413–2423.
19 A. Nel, T. Xia, L. Mädler and N. Li, *Science*, 2006, **311**, 622–627.
20 A. Nemmar, P. H. Hoet, B. Vanquickenborne, D. Dinsdale, M. Thomeer, M. F. Hoylaerts, H. Vanbilloen, L. Mortelmans and B. Nemery, *Circulation*, 2002, **105**, 411–414.
21 G. Oberdörster, E. Oberdörster and J. Oberdörster, *Environ. Health Perspect.*, 2005, **113**, 823–839.
22 P. Carmeliet, *Nat. Med.*, 2003, **9**, 653–660.
23 A. O. Spiel, J. C. Gilbert and B. Jilma, *Circulation*, 2008, **117**, 1449–1459.
24 N. L. Mills, H. Törnqvist, M. C. Gonzalez, E. Vink, S. D. Robinson, S. Söderberg, N. A. Boon, K. Donaldson, T. Sandström, A. Blomberg and D. E. Newby, *N. Engl. J. Med.*, 2007, **357**, 1075–1082.
25 C. A. Pope III, R. T. Burnett, G. D. Thurston, M. J. Thun, E. E. Calle, D. Krewski and J. J. Godleski, *Circulation*, 2004, **109**, 71–77.
26 G. J. Doherty and H. T. McMahon, *Annu. Rev. Biochem.*, 2009, **78**, 857–902.
27 S. D. Conner and S. L. Schmid, *Nature*, 2003, **422**, 37–44.
28 L.-C. Cheng, X. Jiang, J. Wang, C. Chen and R.-S. Liu, *Nanoscale*, 2013, **5**, 3547–3569.
29 C. Foged and H. M. Nielsen, *Expert Opin. Drug Delivery*, 2008, **5**, 105–117.
30 T. Wang, J. Bai, X. Jiang and G. U. Nienhaus, *ACS Nano*, 2012, **6**, 1251–1259.
31 J. Lin and A. Alexander-Katz, *ACS Nano*, 2013, **7**, 10799–10808.
32 A. Verma, O. Uzun, Y. Hu, Y. Hu, H.-S. Han, N. Watson, S. Chen, D. J. Irvine and F. Stellacci, *Nat. Mater.*, 2008, **7**, 588–595.
33 R. R. Arvizo, O. R. Miranda, M. A. Thompson, C. M. Pabelick, R. Bhattacharya, J. D. Robertson, V. M. Rotello, Y. S. Prakash and P. Mukherjee, *Nano Lett.*, 2010, **10**, 2543–2548.
34 U. Taylor, S. Klein, S. Petersen, W. Kues, S. Barcikowski and D. Rath, *Cytometry, Part A*, 2010, **77A**, 439–446.
35 K. Huang, H. Ma, J. Liu, S. Huo, A. Kumar, T. Wei, X. Zhang, S. Jin, Y. Gan, P. C. Wang, S. He, X. Zhang and X.-J. Liang, *ACS Nano*, 2012, **6**, 4483–4493.
36 P. V. Asharani, N. Xinyi, M. P. Hande and S. Valiyaveettil, *Nanomedicine*, 2009, **5**, 51–64.
37 H. Gehrke, J. Pelka, C. Hartinger, H. Blank, F. Bleimund, R. Schneider, D. Gerthsen, S. Bräse, M. Crone, M. Türk and D. Marko, *Arch. Toxicol.*, 2011, **85**, 799–812.
38 S. Bolte and F. P. Cordelieres, *J. Microsc.*, 2006, **224**, 213–232.
39 J. P. Luzio, P. R. Pryor and N. A. Bright, *Nat. Rev. Mol. Cell Biol.*, 2007, **8**, 622–632.
40 S. Fulda, L. Galluzzi and G. Kroemer, *Nat. Rev. Drug Discovery*, 2010, **9**, 447–464.
41 M. P. Murphy, *Biochim. Biophys. Acta*, 2008, **1777**, 1028–1031.
42 K. Kolmakov, V. N. Belov, J. Bierwagen, C. Ringemann, V. Müller, C. Eggeling and S. W. Hell, *Chem. – Eur. J.*, 2010, **16**, 158–166.
43 D. Vercauteren, R. E. Vandenbroucke, A. T. Jones, J. Rejman, J. Demeester, S. C. De Smedt, N. N. Sanders and K. Braeckmans, *Mol. Ther.*, 2010, **18**, 561–569.
44 J. Dausend, A. Musyanovych, M. Dass, P. Walther, H. Schrezenmeier, K. Landfester and V. Mailänder, *Macromol. Biosci.*, 2008, **8**, 1135–1143.

45 J. Blechinger, A. T. Bauer, A. A. Torrano, C. Gorzelanny, C. Bräuchle and S. W. Schneider, *Small*, 2013, **9**, 3970–3980.
46 L. Pelkmans and A. Helenius, *Traffic*, 2002, **3**, 311–320.
47 S. G. Filler, J. N. Swerdloff, C. Hobbs and P. M. Luckett, *Infect. Immun.*, 1995, **63**, 976–983.
48 I. A. Khalil, K. Kogure, H. Akita and H. Harashima, *Pharmacol. Rev.*, 2006, **58**, 32–45.
49 R. G. Parton, B. Joggerst and K. Simons, *J. Cell Biol.*, 1994, **127**, 1199–1215.
50 R. P. Carney, Y. Astier, T. M. Carney, K. Voïtchovsky, P. H. Jacob Silva and F. Stellacci, *ACS Nano*, 2013, **7**, 932–942.
51 G. van Meer, D. R. Voelker and G. W. Feigenson, *Nat. Rev. Mol. Cell Biol.*, 2008, **9**, 112–124.
52 C. Westerhausen, F. G. Strobl, R. Herrmann, A. T. Bauer, S. W. Schneider, A. Reller, A. Wixforth and M. F. Schneider, *Biophys. J.*, 2012, **102**, 1032–1038.
53 M. P. Monopoli, C. Aberg, A. Salvati and K. A. Dawson, *Nat. Nanotechnol.*, 2012, **7**, 779–786.
54 P. R. Leroueil, S. Hong, A. Mecke, J. R. Baker, B. G. Orr and M. M. Banaszak Holl, *Acc. Chem. Res.*, 2007, **40**, 335–342.
55 T. Yu, J. Zeng, B. Lim and Y. Xia, *Adv. Mater.*, 2010, **22**, 5188–5192.
56 Q. Wang, W. Jia, B. Liu, W. Zhao, C. Li, J. Zhang and G. Xu, *Chem. – Asian J.*, 2012, **7**, 2258–2267.
57 J. Blechinger, R. Herrmann, D. Kiener, F. J. García-García, C. Scheu, A. Reller and C. Bräuchle, *Small*, 2010, **6**, 2427–2435.
58 J. Schindelin, I. Arganda-Carreras, E. Frise, V. Kaynig, M. Longair, T. Pietzsch, S. Preibisch, C. Rueden, S. Saalfeld, B. Schmid, J.-Y. Tinevez, D. J. White, V. Hartenstein, K. Eliceiri, P. Tomancak and A. Cardona, *Nat. Methods*, 2012, **9**, 676–682.